Controlled generation of intrinsic localized modes in microelectromechanical cantilever arrays

Qingfei Chen,[1] Ying-Cheng Lai,[1,2] and David Dietz[3]
[1]*School of Electrical, Computer, and Energy Engineering, Arizona State University, Tempe, Arizona 85287, USA*
[2]*Department of Physics, Arizona State University, Tempe, Arizona 85287, USA*
[3]*Air Force Research Laboratory, AFRL/RDHE, 3550 Aberdeen Ave. SE, Kirtland AFB, New Mexico 87117, USA*

(Received 25 July 2010; accepted 24 November 2010; published online 29 December 2010)

We propose a scheme to induce intrinsic localized modes (ILMs) at an *arbitrary* site in microelectromechanical cantilever arrays. The idea is to locate the particular cantilever beam in the array that one wishes to drive to an oscillating state with significantly higher amplitude than the average and then apply small adjustments to the electrical signal that drives the whole array system. Our scheme is thus a global closed-loop control strategy. We argue that the dynamical mechanism on which our global driving scheme relies is spatiotemporal chaos and we develop a detailed analysis based on the standard averaging method in nonlinear dynamics to understand the working of our control scheme. We also develop a Markov model to characterize the transient time required for inducing ILMs. © *2010 American Institute of Physics*. [doi:10.1063/1.3527008]

In a variety of spatially extended physical systems, intrinsic localized modes (ILMs) can arise. Associated with such a motion, a few elements in the system oscillate with significantly larger amplitudes than those of the vast majority of the remaining elements. A few years ago, it was experimentally found that ILMs can occur in microelectromechanical (MEM) cantilever-array systems. The specific locations of the ILMs in the MEM array system are, however, unpredictable due to the intrinsic symmetry of the system. An interesting question is thus whether it would be feasible to derive a suitable control scheme to excite an ILM at a desirable target location without individual actuation access to the specific cantilever. Recently, we addressed this question by outlining an idea of applying global frequency-modulation control to MEM oscillator array systems. A key requirement of our control method is that the system exhibit spatiotemporal chaos, which is, however, ubiquitous in driven MEM cantilever-array systems. As a chaotic state contains an infinite number of unstable motions including ILMs, a suitable control can be used to stabilize any target ILM. In this paper, we present a detailed analysis of our spatiotemporal-chaos based global control method to induce ILMs in MEM array systems. In particular, we first derive stability conditions for localized vibration modes in weakly coupled MEM cantilever arrays. We then perform a dynamical analysis of the control process, which reveals the physical mechanism underpinning the control. Finally, we identify three backbone dynamical states and derive a corresponding Markov-transition model to analyze the issue of transient time required for achieving the control. We show that during the control process, the system switches between a spatiotemporal chaotic state and a low-energy state in which all cantilevers oscillate with near zero amplitude. The system can then be stabilized once its state matches the spatial pattern of the desired ILM. Our work illustrates that the principle of chaos control can be applied to achieve desirable system performance in spatially extended physical systems of significant recent interest.

I. INTRODUCTION

The phenomenon of nonlinear energy localization in spatially extended physical systems has attracted continuous interest from various branches of physics.[1–4] For example, such dynamical states, called *intrinsic localized modes* (ILMs), can occur in a defect-free nonlinear lattice, extending over only a few lattice sites. The physical systems where ILMs have been studied include Josephson junctions,[5] optical waveguide arrays,[6] photonic crystals,[7] antiferromagnets,[8] Bose–Einstein condensates (BECs) in optical lattices,[9–14] and more recently, microelectromechanical (MEM) oscillator arrays.[15] Take BECs as an example to illustrate the intensive interest in this topic. The existence of periodic localized oscillations of two coupled condensates was predicted in Ref. 9. Three coupled BECs were considered in Ref. 10 and the existence of ILMs in one-dimensional BEC arrays was discussed in Ref. 11. In Ref. 16, ILM phenomena were reported in dilute BECs trapped in a periodic potential regardless of whether the interatomic potential is attractive or repulsive. The existence of localized modes associated with quasi-one-dimensional BECs confined in periodic potentials was demonstrated in Ref. 12. It was also theoretically predicted[13] that ILMs can exist in atomic-molecular BECs trapped in an optical lattice. In Ref. 14, localization phenomenon of BECs in optical lattices was shown to be generated by boundary dissipations.

The focus of this paper is on ILMs in MEM oscillator arrays, an area of research that started around 2003.[17] The seminal work in Ref. 17 laid the foundation for observing

ILMs in MEM systems[18] that have been researched intensively in applied physics and engineering, and have been implemented in all kinds of technological devices. From the standpoint of dynamics, MEM oscillator arrays are nonlinear, spatially extended dynamical systems. Indeed, a recent work demonstrated that under fairly general conditions, spatiotemporal chaos can arise in such systems and, interestingly, the chaotic state can act as a precursor or platform for generating ILMs.[19] In a typical experimental setting,[17] ILMs can be generated at random sites by chirping the frequency of the external driving signal. A question then concerns whether it is feasible to derive a suitable control scheme to excite an ILM at an *arbitrary target location*. Intuitively, this can be done by using local driving (pinning). In this regard, it was demonstrated experimentally[20] that the pinning method can indeed induce ILMs, where a laser beam was employed to trap ILM at a target location through localized thermal-mechanical effect. A question is then whether an alternative *global* control scheme can be devised to achieve the goal of exciting ILM at any desirable location in the MEM array. In a recent Letter,[21] we demonstrated that such a control scheme is indeed possible through the method of frequency modulation to generate spatiotemporal chaos as a stepping stone to ILMs.

The reasons that we focus on chaos as a precursor for ILMs are as follows. The discovery that spatiotemporal chaos can facilitate the generation of ILMs in physical systems (other than MEM oscillator arrays)[22,23] and the demonstration of this phenomenon in MEM oscillator arrays[19] suggest the feasibility of using global driving to excite ILMs. In particular, a spatiotemporally chaotic state contains an infinite number of modes of motion, including various ILMs, all unstable. In a MEM oscillator array, spatiotemporal chaos is pervasive and can be realized readily by adjusting the frequency of the driving.[19] When the system is in spatiotemporal chaos, ILMs at all possible locations have been embedded in the chaotic state, although they are unstable. Since spatiotemporal chaos occurs globally in the entire oscillator-array system, it is, in principle, possible to articulate small, judiciously chosen, and time-dependent driving to excite an ILM at any desirable location.[24]

The basic idea of our control method is shown schematically in Fig. 1. We first set the frequency of the external driving so that the MEM oscillator array system exhibits spatiotemporal chaos, which provides the necessary condition for generating ILMs, i.e., spatial heterogeneity. Assume that a time series, typically the displacement signal, at the target site can be measured. (For example, an image sensor can be used for scanning the cantilever beam movements at the surface of the MEM lattice.[15]) We then use the time series as input in a feedback scheme for tuning the global driving frequency, stabilizing the particular ILM for that beam.

In this paper, we provide a detailed analysis of our spatiotemporal-chaos based global control method to induce ILMs in MEM array systems. New results beyond those in our Letter[21] include a comprehensive treatment of the nonlinear dynamics of the MEM array system, a detailed derivation of the control law based on the dynamics, and the result on the average transient time to achieve the control. In Sec. II, we describe our driving scheme. The dynamical mechanism of ILMs in MEM oscillator arrays and the working of our scheme are analyzed in Sec. III. Transient-time analysis is presented in Sec. IV. A conclusion is given in Sec. V.

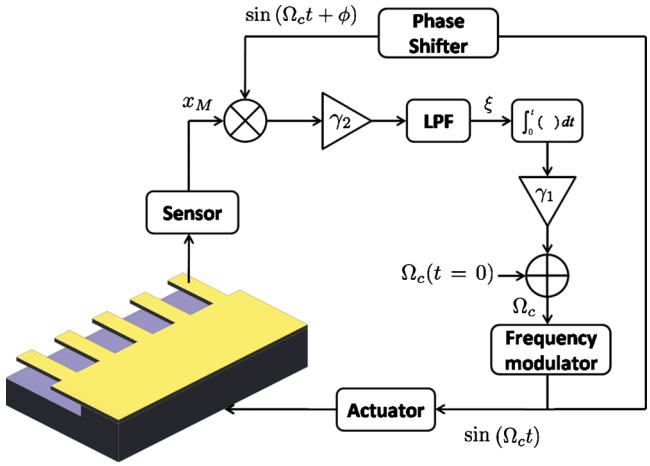

FIG. 1. (Color online) Illustration of our scheme of global control to excite a particular ILM in a MEM oscillator-array system.

II. FREQUENCY-MODULATION CONTROL OF ILMs

A. Controller design

Although we shall demonstrate our idea using MEM oscillator array systems, the dynamics of ILMs are representative of a broader class of physical systems. We thus expect our result to provide insights into the dynamics of ILMs in general.

The dynamics of a MEM cantilever array can be described by coupled driven Duffing oscillators,[17]

$$m_i\ddot{x}_i + b_i\dot{x}_i + k_{2i}x_i + k_{4i}x_i^3 + k_I(2x_i - x_{i+1} - x_{i-1}) = m_i\alpha\cos(\Omega t), \quad (1)$$

where x_i $(i=1,\ldots,N)$ is the displacement of the end point of the ith cantilever beam of effective mass m_i, b_i is the damping coefficient, k_{2i} and k_{4i} are the on-site harmonic and quadratic spring constants of the ith beam, respectively, and k_I is the harmonic coupling spring constant. Each beam is subject to a common sinusoidal driving of acceleration α and angular frequency Ω. Equation (1), in fact, models a nonlinear dynamical system that arises commonly in a variety of physical and engineering situations. For appropriately strong driving, each oscillator can exhibit a bistable behavior with two possible states: one of low and another of high amplitude (energy). An ILM is a state where the amplitudes of a few oscillators are high but the remaining majority of oscillators are in the low-energy state.

The displacement of the ith oscillator, in general, can be written as

$$x_i(t) = U_i(t)\cos(\Omega t) - V_i(t)\sin(\Omega t) \equiv r_i(t)\cos[\Omega t + \theta_i(t)], \tag{2}$$

where $r_i = \sqrt{U_i^2 + V_i^2}$ and θ_i are the radial and angular coordinates of (U_i, V_i), respectively. When the driving frequency Ω is close to the resonant frequency and the driving amplitude is relatively strong, the beam dynamics is typically bistable. In this regime, for the low-energy state, the phase angle $\theta_i(t)$ is usually stabilized about a value less than $-\pi/2$, but for the high-energy state, the stable phase value is larger than $-\pi/2$.[25,26]

Our proposed control scheme is illustrated in Fig. 1. We first tune the frequency of the external driving so that the MEM oscillator array system exhibits spatiotemporal chaos. We then employ a displacement sensor to acquire the oscillation signal of a desirable beam M about which ILM is to be generated. The signal is multiplied by a sinusoidal signal of the controlled frequency and reference phase angle ϕ. The combined signal is led to pass through a low-pass filter (LPF) so that the phase information can be extracted. Finally, the signal is integrated to tune the controlled frequency Ω_c. The mathematical equations modeling this frequency modulator are

$$\begin{cases} \dot{\Omega}_c = \gamma_1 \xi \\ \dot{\xi} = -\dfrac{1}{\tau}[\xi + \gamma_2 x_M \sin(\Omega_c t + \phi)], \end{cases} \tag{3}$$

where Ω_c is the time-dependent driving frequency, ξ is a variable related to the phase-angle difference, τ is the typical time corresponding to the cut-off frequency of the LPF, and γ_1 and γ_2 are the gains of the modulator. The equations for the MEM cantilever-array system under the controlled driven frequency thus become

$$m_i\ddot{x}_i + b_i\dot{x}_i + k_{2i}x_i + k_{4i}x_i^3 + k_I(2x_i - x_{i+1} - x_{i-1}) = m_i\alpha\cos(\Omega_c t). \tag{4}$$

In Eq. (3), the value of $2\pi/\tau$ should be set to be much smaller than Ω_c so that the high-frequency component in $\gamma_2 x_M \sin(\Omega_c t + \phi)$ can be filtered out. In a stable modulation state, Ω is locked to Ω_c and the multiplication term $x_M \sin(\Omega_c t + \phi)$ is decoupled as

$$x_M \sin(\Omega_c t + \phi) = \frac{r_M(t)}{2}\{\sin(2\Omega_c t + \theta_M(t) + \phi) + \sin[\phi - \theta_M(t)]\}.$$

By setting $2\pi/\tau \ll \Omega_c$, the term $\sin[2\Omega_c t + \theta_M(t) + \phi]$ whose frequency is $2\Omega_c$ can be filtered out. Thus, the system variable $\xi(t)$ is modulated by the phase-angle difference between the output and the reference values. We have

$$\xi(t) \approx \gamma_2 \frac{r_M(t)}{2}\sin[\theta_M(t) - \phi]. \tag{5}$$

As a result, the differential equation governing the change in the modulated angular frequency is approximately

$$\dot{\Omega}_c(t) = \gamma_1\xi(t) \approx \frac{\gamma_1\gamma_2}{2} r_M(t)\sin[\theta_M(t) - \phi]. \tag{6}$$

The output phase angle can thus be stabilized around the desired reference value that corresponds to the high-energy oscillation state at site M. In a single cantilever system, the maximum high-energy state has the phase angle of $-\pi/2$ (see the Appendix). In the coupled cantilever arrays system, we find that the phase angle of the high-energy state is also close to this value, suggesting that one can directly set the angle value ϕ close to $-\pi/2$ to achieve the desired control performance.

B. Stability analysis

We now address the stability issue of our proposed control scheme. We first consider the situation of the decoupled limit defined by $k_I = 0$. With the target cantilever equation and the controller expressed by Eq. (3), the whole controlled MEM array system can be described by

$$m\ddot{x} + b\dot{x} + k_2 x + k_4 x^3 = m\alpha\cos(\Omega_c t),$$

$$\dot{\Omega}_c = \gamma_1\xi,$$

$$\dot{\xi} = -(1/\tau)[\xi + \gamma_2 x\sin(\Omega_c t + \phi)]. \tag{7}$$

If Ω_c is close to the natural frequency $\Omega_0 = \sqrt{k_2/m}$, which holds when Ω_c is chosen to be in the bistable region, one can apply the invertible van der Pol transformation to system (7),

$$\begin{pmatrix} u \\ v \end{pmatrix} = A\begin{pmatrix} x \\ \dot{x} \end{pmatrix}, \tag{8}$$

where

$$A = \begin{pmatrix} \cos\Omega_c t & -\sin\Omega_c t/\Omega_c \\ -\sin\Omega_c t & -\cos\Omega_c t/\Omega_c \end{pmatrix}.$$

The transformed system is

$$\frac{du}{dt} = \frac{1}{\Omega_c}\Big[(k_2/m - \Omega_c)(u\cos\Omega_c t - v\sin\Omega_c t) - \frac{b}{m}\Omega_c(u\sin\Omega_c t + v\cos\Omega_c t) + \frac{k_4}{m}(u\cos\Omega_c t - v\sin\Omega_c t)^3 - \alpha\cos\Omega_c t\Big]\sin\Omega_c t,$$

$$\frac{dv}{dt} = \frac{1}{\Omega_c}\Big[(k_2/m - \Omega_c)(u\cos\Omega_c t - v\sin\Omega_c t) - \frac{b}{m}\Omega_c(u\sin\Omega_c t + v\cos\Omega_c t) + \frac{k_4}{m}(u\cos\Omega_c t - v\sin\Omega_c t)^3 - \alpha\cos\Omega_c t\Big]\cos\Omega_c t,$$

$$\frac{d\Omega_c}{dt} = \gamma_1\xi,$$

$$\frac{d\xi}{dt} = -\frac{\xi}{\tau} - \frac{\gamma_2}{\tau}(u\cos\Omega_c t - v\sin\Omega_c t)\sin(\Omega_c t + \phi). \quad (9)$$

Averaging the system (9) over one time period $T=2\pi/\Omega_c$ and transforming the averaged system into the polar coordinates $[r,\theta|r=\sqrt{u^2+v^2},\ \theta=\arctan(v/u)]$, we obtain the following averaged system:

$$\frac{dr}{dt} = \frac{1}{2\Omega_c}\left[-\frac{\Omega_c b r}{m} - \alpha\sin\theta\right],$$

$$\frac{d\theta}{dt} = \frac{1}{2\Omega_c r}\left[(k_2/m - \Omega_c^2)r + \frac{3k_4 r^3}{4m} - \alpha\cos\theta\right],$$

$$\frac{d\Omega_c}{dt} = \gamma_1\xi,$$

$$\frac{d\xi}{dt} = -\frac{\xi}{\tau} - \frac{\gamma_2}{\tau}\sin(\phi-\theta). \quad (10)$$

In system (10), there is only one equilibrium given by

$$\begin{pmatrix} r \\ \theta \\ \Omega_c \\ p \end{pmatrix} = \begin{pmatrix} -[(m\alpha)/(\Omega_c b)]\sin\phi \\ \phi \\ F(\phi) \\ 0 \end{pmatrix}, \quad (11)$$

where $F(\phi)=\sqrt{k_2/m+3k_4r^2/(4m)+\alpha\cos\phi}$ is ultimately a function of Ω_c since the variable ϕ is related to Ω_c as

$$\left(\frac{3k_4m^2\alpha^3}{4b^3} - \frac{\Omega_c^2(m\Omega_c^2-k_2)\alpha}{b}\right)\tan\phi^3 + \Omega_c^3\alpha\tan\phi^2 - \frac{\Omega_c^2(m\Omega_c^2-k_2)\alpha}{b}\tan\phi + \Omega_c^3\alpha = 0, \quad (12)$$

Equation (12) is derived from Eq. (10) by setting the right-hand sides to zero.

The Jacobian matrix of the system (10) evaluated at the equilibrium solution (11) is

$$\begin{pmatrix} -\frac{b}{2m} & -\frac{\alpha}{2\Omega_c}\cos\phi & \frac{\alpha}{2\Omega_c^2}\sin\phi & 0 \\ \Delta_1 & -\frac{b}{2m} & \Delta_2 & 0 \\ 0 & 0 & 0 & \gamma_1 \\ 0 & \frac{\gamma_2 m\alpha\sin\phi}{2\tau F(\phi)b} & 0 & -\frac{1}{\tau} \end{pmatrix}, \quad (13)$$

where

$$\Delta_1 = 3k_4\alpha/(4\Omega_c^2 b)\sin\phi,$$

$$\Delta_2 = -1/2 - k_2/(2\Omega_c^2 m) - 3k_4\alpha^2 m/(8\Omega_c^4 b^2)\sin^2\phi - b/(2m\Omega_c)\tan^{-1}\phi.$$

The characteristic equation of Eq. (13) can be obtained as

$$\lambda^4 + a_1\lambda^3 + a_2\lambda^2 + a_3\lambda^1 + a_4 = 0, \quad (14)$$

where the parameters a_1–a_4 are

$$a_1 = \frac{b}{m} + \frac{1}{\tau}, \quad (15)$$

$$a_2 = \frac{b^2}{4m^2} + \frac{b}{m\tau} + \frac{\alpha\Delta_1\cos\phi}{2\Omega_c},$$

$$a_3 = \frac{1}{\tau}\left(\frac{b^2}{4m^2} + \frac{\alpha}{2\Omega_c}\Delta_1\cos\phi + \frac{\gamma_1\gamma_2 m\alpha}{2F(\phi)b}\Delta_2\sin\phi\right),$$

$$a_4 = \frac{1}{\tau}\left(\frac{\gamma_1\gamma_2\alpha}{4F(\phi)}\Delta_2\sin\phi + \frac{\gamma_1\gamma_2 m\alpha^2}{4F(\phi)b\Omega_c^2}\sin^2\phi\right). \quad (16)$$

Note that all parameters are positive. This is because, as we set ϕ close to the value that corresponds to the highest energy state, $-\pi/2$, we have $\sin\phi<0$, $\cos\phi\approx 0$, and $\tan^{-1}\phi\approx 0$. We thus have $\Delta_1>0$ and $\Delta_2<0$. As a result, we have $a_1,a_2,a_3,a_4>0$. The Routh–Hurwitz condition for stability[27] is

$$A_1 = a_1 > 0,$$

$$A_2 = a_1a_2 - a_3 > 0,$$

$$A_3 = a_1a_2a_3 - a_3^2 - a_1^2a_4 > 0,$$

$$A_4 = a_1a_4A_3 > 0. \quad (17)$$

Since a_1–a_4 are all positive, the stability condition (17) can be simplified as

$$A_2 = a_1a_2 - a_3 > 0,$$

$$A_3 = a_1a_2a_3 - a_3^2 - a_1^2a_4 > 0. \quad (18)$$

For the case of weakly coupled cantilever arrays, due to the high localized energy at the target cantilever (in ILM state), we have $x_M \gg x_{M+1}, x_{M-1}$ for the coupling term in Eq. (4). The stability condition (18) thus holds for weakly coupled cantilever-array system as well. We mention that the above analysis is valid only for the local stability of the ILM state. To make the system eventually settle into the desired ILM state, a number of other conditions are needed in addition to the local stability criterion. These will be detailed in Sec. III B.

C. Simulation results

Examples illustrating our scheme to induce ILMs are shown in Figs. 2(a)–2(d) in which the fourth-order Runge–Kutta method with a time step of 6.4×10^{-5} s is employed to integrate the dynamical equations. The coupled MEM oscillator system consists of two groups of beams of different length, arranged alternatively in space. The cantilevers are coupled by an overhang. The structural parameters of the system are chosen according to their respective experimental values[17] $(m_i,b_i,k_{2i},k_{4i})=(5.46\times10^{-13}\ \text{kg}, 6.24\times10^{-11}\ \text{kg/s}, 0.303\ \text{N/m}, 5\times10^{8}\ \text{N/m}^3)$ for odd i, the long beams, and $(m_i,b_i,k_{2i},k_{4i})=(4.96\times10^{-13}\ \text{kg}, 5.67\times10^{-11}\ \text{kg/s}, 0.353\ \text{N/m}, 5\times10^{8}\ \text{N/m}^3)$ for even i, the short beams. The parameters of the driving are chosen to be $(\alpha,\gamma_1,\gamma_2,\tau)=(1.56\times10^{4}\ \text{m/s}^2, 5, 10^{12}, 0.1361\ \text{s})$.

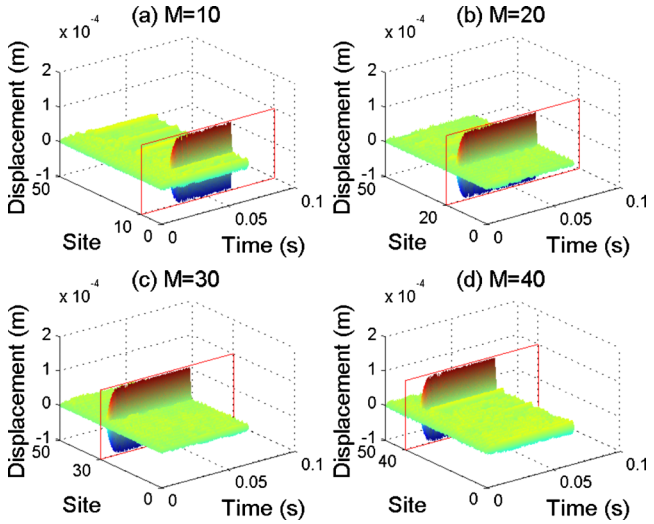

FIG. 2. (Color online) For a MEM oscillator system of $N=50$ beams of alternating length, space-time plots of four examples of inducing ILMs at sites $M=10$ (a), 20 (b), 30 (c), and 40 (d). The initial value of Ω_c is $\Omega_c(t=0)=9.24\times10^5$ rad/s. Dark lines indicate higher amplitudes. See text for various parameters.

We have simulated an oscillator array of $N=50$ beams, where the phase in Eq. (3) is set to be $\phi=-\pi/2$. The initial value of the driving frequency is set to be $\Omega_c(t=0)=9.24\times10^5$ rad/s so that the system exhibits spatiotemporal chaos (Sec. III). The initial displacements and velocities of all the beams are set to be zero. The four panels in Figs. 2(a)–2(d) correspond to the cases where an ILM has been induced at site $M=10$, 20, 30, and 40, respectively. Apparently, our method is capable of inducing robust ILMs at any desirable site in the system. Since the device model and parameters are from experiments[17] where the MEM array system consists of multiple bielement cells and each cell is a dual coupled beam with different beam lengths, ILMs can be induced only around the shorter beam in each bielement cell, namely, those beams with even sequence numbers.

III. DYNAMICAL MECHANISM OF CONTROLLED GENERATION OF ILMS

A. Dynamical mechanism of frequency-modulation control

To understand the working mechanism of our scheme, it is insightful to explore the dynamical mechanism for ILMs to arise naturally (without any control) in a MEM oscillator-array system. We start with the system [Eq. (1)] in its nominal setting, i.e., the driving frequency Ω does not depend on time. While the dynamical solutions of ILMs in conservative systems have been understood reasonably well,[28,29] systems of MEM oscillator arrays are typically dissipative. For a coupled Duffing oscillator array with large nonlinearity, multiple stable solutions may coexist. (The issue of multistability in coupled cantilever arrays was discussed briefly in Ref. 30.) To understand the phenomenon of multistability, we use the standard averaging method.[31] Inserting Eq. (2) into Eq. (1) and taking the time average in one driving period $2\pi/\Omega$, we obtain the following averaged system:

$$\frac{du_i}{dt}=\frac{1}{2\Omega}\left[(\Omega^2-\Omega_{0i}^2)v_i-\frac{3}{4}\frac{k_{4i}}{m_i}v_i(u_i^2+v_i^2)-\frac{\Omega_{0i}}{Q_i}\Omega u_i - \frac{k_I}{m_i}(2v_i-v_{i+1}-v_{i-1})\right],$$

$$\frac{dv_i}{dt}=\frac{1}{2\Omega}\left[-(\Omega^2-\Omega_{0i}^2)u_i+\frac{3}{4}\frac{k_{4i}}{m_i}u_i(u_i^2+v_i^2)-\frac{\Omega_{0i}}{Q_i}\Omega v_i - \alpha+\frac{k_I}{m_i}(2u_i-u_{i+1}-u_{i-1})\right],\quad i=1,\ldots,N, \tag{19}$$

where $Q_i=\sqrt{m_ik_{2i}}/b_i$ is the quality factor, $\Omega_{0i}=\sqrt{k_{2i}/m_i}$ is the resonant frequency of the ith beam, and $u_i(t)$ and $v_i(t)$ are the averaged functions of $U_i(t)$ and $V_i(t)$, respectively. Here, we consider the typical experimental setting[17] where k_I is fixed (e.g., $k_I=0.0241$ N/m) and the driving frequency Ω can be varied.

The boundaries of multiple dynamical states can be obtained by examining the bifurcation points in Eq. (19). In particular, we can continue the dynamical solutions from the decoupled limit $k_I=0$ to $k_I=0.0241$ N/m (the effective coupling spring constant[15]) and locate the bifurcation point in Ω (boundary).[32] The boundaries between spatiotemporal chaotic states (denoted as SC) and the low-energy states (denoted as LES) are denoted by Ω_B^{SC} and those between SC states and ILM states are denoted by Ω_B^{ILM}. In the region $\Omega_C<\Omega_B^{\mathrm{SC}}$, the MEM cantilever arrays system is in some SC state and, in the region $\Omega_C>\Omega_B^{\mathrm{ILM}}$, the system is likely to be stabilized around an ILM state. In the intermediate region $(\Omega_B^{\mathrm{SC}}<\Omega_C<\Omega_B^{\mathrm{ILM}})$, the system can be in some LES state only.

Since frequency modulation is directly controlled by the difference between the real-time phase angle and its reference value, a key quantity in the controlled regime is the ranges of phase angles in different dynamical states. Our idea is to examine the relationship between θ_M and r_M in the decoupled limit and then use the obtained relation to heuristically explain the phase angles' ranges. For the Mth beam, in the decoupled limit $(k_I=0)$ the input energy in one driving period from the external driving force is

$$\varepsilon_{\mathrm{in}}=\int_x m_M\alpha\cos(\Omega t)dx_M. \tag{20}$$

Since $x_M(t)=r_M\cos(\Omega t+\theta_M)$, where the rates of change in $r_M(t)$ and $\theta_M(t)$ are much smaller than that of $\Omega(t)$, we can regard the amplitude and the phase angle as being constants in a driving period. We thus have

$$\varepsilon_{\mathrm{in}}\approx\int_{2k\pi/\Omega}^{2(k+1)\pi/\Omega} m_M\alpha\cos(\Omega t)(-\Omega r_M)\sin(\Omega t+\theta_M)dt = -2\pi m_M\alpha r_M\sin(\theta_M). \tag{21}$$

From Eq. (21), we see that the phase angle θ_M is confined in the region $(-\pi,0)$ since the energy input is always positive for a stable damped oscillatory system. Similarly, the dissipated energy due to the damping force is

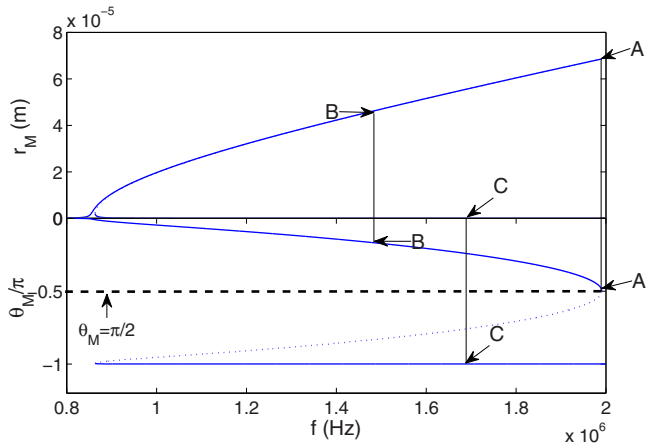

FIG. 3. (Color online) Frequency dependence of oscillation amplitude r_M and phase angle θ_M in the decoupled limit of $k_I=0$.

$$\varepsilon_{\text{out}} = \int_x b\dot{x}_M dx_M \approx \int_{2k\pi/\Omega}^{2(k+1)\pi/\Omega} b[\Omega r_M \sin(\Omega t + \theta_M)]^2 dt$$
$$= \pi b \Omega r_M^2. \tag{22}$$

Energy conservation requires

$$\varepsilon_{\text{in}} = \varepsilon_{\text{out}}, \tag{23}$$

which leads to the following formula relating the average phase angle to the average amplitude and the driving frequency:

$$\sin(\theta_M) = -\frac{b}{2\alpha m_M}\Omega r_M = -\frac{r_M}{r_M^{\max}}, \tag{24}$$

where $r_M^{\max}=2\alpha m_M/(b\Omega)$ is the oscillation amplitude of the resonant peak. In Eq. (24), since r_M and $r_M^{\max}$ are both positive, θ_M is confined in the range of $(-\pi,0)$. The amplitude r_M is confined in the region $(0,r_M^{\max})$. The frequency dependence of r_M and θ_M is shown in the upper and lower panels of Fig. 3.

From Eq. (24), it can be seen that the state with the maximum oscillation amplitude $r_M^{\max}$ (denoted as "A" in Fig. 3) has the phase angle of $-\pi/2$. Moreover, there are two branches of stable motion: one of large and another of small oscillation amplitude. Furthermore, in the lower panel, we see that the high-amplitude branch has phase angle larger than $-\pi/2$ $(0>\theta_M^h>-\pi/2)$ and the low-energy one has phase angle smaller than $-\pi/2$ $(-\pi<\theta_M^l<-\pi/2)$.

The results obtained from the decoupled limit can shed light on the phase-angle property of dynamical states in coupled system (1). Since in a spatiotemporal chaotic state every site has moderate energy,[33] the Mth beam's oscillation can be heuristically treated as in the high-energy branch in Fig. 3 and its phase angle is larger than $-\pi/2$ (labeled as "B" in the figure). On the other hand, the low-energy state of the Mth beam can be regarded as in the low-energy branch in Fig. 3 (labeled as "C"). Since the reference phase angle ϕ is set to be close to $-\pi/2$, we have

$$\begin{cases} \bar{\theta}_M|_{\text{SC}} - \phi > 0 \\ \bar{\theta}_M|_{\text{LES}} - \phi < 0, \end{cases} \tag{25}$$

where $\bar{\theta}_M$ denotes the average value of θ_M. Consequently, the value of

$$\Theta_M := r_M \sin(\theta_M - \phi), \tag{26}$$

which governs the frequency-varying rate, as shown in Eq. (6), will change sign from that associated with an SC state to an LES state. The system of MEM cantilever array [Eq. (1)] has been numerically computed and the average values of Θ_M in different dynamical regimes are obtained in Ref. 19. The results of phase angles and frequency-modulation properties are summarized in Table I, where the simulated values agree with those from the stability analysis.

The above analysis suggests a general strategy for inducing ILMs in a MEM oscillator-array system. To explain the strategy, it is necessary to reveal the detailed dynamics of the control and of the cantilever array. An example is shown in Fig. 4 where the underlying system has $N=128$ beams (64 cells) and the desirable site for ILM is $M=64$. When the system is in the spatiotemporal-chaos regime, $\dot{\bar{\Omega}}_c>0$ so that the frequency will increase and exceed Ω_B^{SC}, which is indicated in Fig. 4(c). If the system cannot get into the basin of a high-energy mode (ILM), it will go to the basin of a low-energy state. If this happens, $\dot{\bar{\Omega}}_c$ will become negative, reducing the driving frequency. As a result, if ILM does not occur, the modulated driving frequency Ω_c will switch back and forth between some values in the chaotic and in the low-energy regimes [Fig. 4(c)]. This process is denoted as the selecting phase in Fig. 4, during which the value of $\bar{\Theta}_M$ changes constantly. There is then a nonzero probability for the system to get into an ILM state, which is the locking phase in Fig. 4. In the locking phase, the modulating frequency $\Omega_c(t)$ increases with time, approaching asymptoti-

TABLE I. Dynamical, phase, and frequency-modulation properties of MEM cantilever arrays (1) in different dynamical regimes for $k_I=0.0241$ N/m, where $\Omega_B^{\text{SC}}\approx 9.254\times 10^5$ rad/s is the boundary between SC and LES and $\Omega_B^{\text{ILM}}\approx 9.312\times 10^5$ rad/s is the boundary between LES and ILM states (Ref. 19).

Frequency range	$\Omega_C<\Omega_B^{\text{SC}}$	$\Omega_B^{\text{SC}}<\Omega_C<\Omega_B^{\text{ILM}}$	$\Omega_C>\Omega_B^{\text{ILM}}$
Dynamical regime	SC	LES	ILMs
Phase property	$\bar{\theta}_M>-\frac{\pi}{2}$ [a]	$\theta_M<-\frac{\pi}{2}$ [a]	θ_M is close to $-\frac{\pi}{2}$ at ILM
Frequency-modulation property	$\dot{\bar{\Omega}}_c>0$	$\dot{\bar{\Omega}}_c<0$	$\dot{\bar{\Omega}}_c\approx 0$ at ILM

[a]Reference 21.

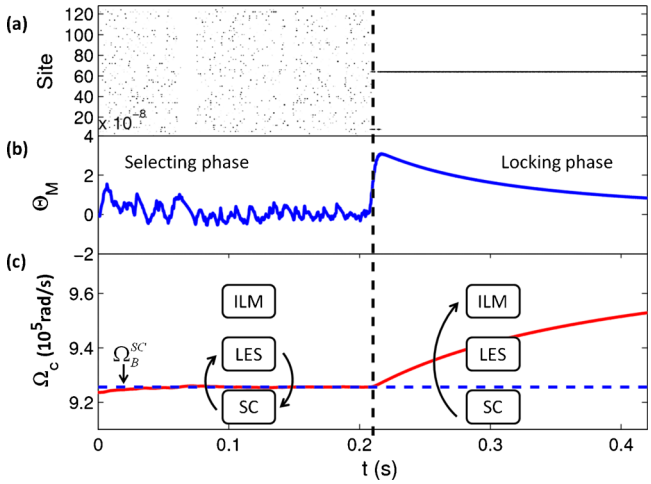

FIG. 4. (Color online) For a MEM oscillator system of $N=128$ beams, an example of stabilizing an ILM at site $M=64$. (a) Space-time plot of beam amplitude. (b) Time series of the phase difference $\Theta_M(t)$ for $M=64$. The initial value of Ω_c is set to be $\Omega_c(t=0)=9.24\times10^5$ rad/s. The vertical dashed line at $t\approx0.21$ s denotes the boundary between the selecting and the locking phase. (c) Time series of the modulating frequency $\Omega_c(t)$. Ω_B^{SC} is the boundary between SC and LES states.

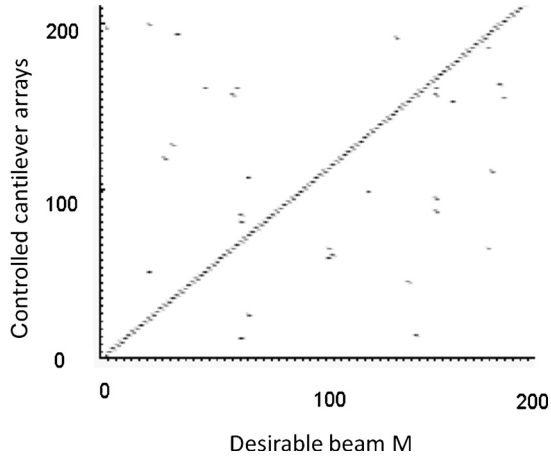

FIG. 5. Controlled system states for the case of 200 MEM cantilevers. Each column in the figure denotes the arrays' controlled state for a specific desirable site (its x values). The initial condition of the simulation is identical for each M.

cally a constant value as the ILM state becomes stable [Fig. 4(c)]. When this occurs, $\bar{\Theta}_M$ is maintained at a positive value but it decreases slowly as the system evolves into a stable ILM state defined by $\theta_M=\phi$, as shown in Fig. 4(b). Due to the relatively small basin of attraction of the high-energy state in a single driven Duffing oscillator in the bistability regime,[19] the probability of generating an ILM through random-phase changes is typically small, leading to a relatively long period of transient phase before ILM is actually realized. Once a particular oscillator has been locked in an ILM state, the random fluctuations in $\bar{\Theta}_M$ are reduced significantly [Fig. 4(b)], preventing the oscillators at other sites to enter some ILM states.

This mechanism also suggests that our approach to inducing ILM can be successful even when the initial value of the driving frequency Ω_c falls outside the regime of spatiotemporal chaos. In particular, if the initial $\Omega_c(t=0)$ is above Ω_B^{SC}, the system will converge to a low-energy state that is always stable, insofar as the condition $\Omega_c>\Omega_B^{SC}$ is satisfied. As a result, Θ_M will become negative, making $\dot{\bar{\Omega}}_c<0$. The value of the driving frequency will consequently be tuned to that in the spatiotemporal chaos regime again, "preparing" the system for excitation into some desirable ILM states.

We note that, although the small basin of attraction of the ILM states makes the probability of creating ILMs at other sites small, for a large-size array, there is a possibility that some ILMs at other sites can be simultaneously locked together with the one at the target site. Figure 5 shows the controlled state in a system of 200 MEM cantilevers. In the figure, each column represents the controlled system state for a specific target site M (its x value). The result demonstrates that ILMs at other sites can indeed be excited. However, since the spatiotemporal chaotic state, which is the platform of ILM control, is sensitive to the initial condition, the control result will depend on the initial dynamical state of the array system. Thus, if multiple ILMs occur in the controlled system, one can restore the system to spatiotemporal chaotic state (by disabling the controller and then reducing the driven frequency) and repeat the control process several times until the desired ILM pattern is created without any other ILMs in the system.

B. Strategy of choosing control parameters

For the controller design [Eq. (3)], the values of the parameters τ, γ_1, and γ_2 should be chosen in the region determined by the local stability condition [Eq. (18)]. Our stability analysis indicates that the controller utilizes the phase characteristics of different dynamical states and the frequency modulation is triggered by a "seed" small-amplitude ILM provided by spatiotemporal chaos, which can be amplified into a large, stable ILM state at the desirable site. Specifically, the frequency ramping can gradually move the ILM states in the phase space and their basin of attraction. The moving basin attracts and pulls the system state to the final, desirable ILM state associated with the phase $\theta_M=\phi$. However, the nonstationary, small-amplitude ILM states can also change the localized energy. As a result, control may be lost. The implication is that, besides the local stability condition analyzed in Sec. II B, three extra conditions are necessary to make the control scheme successful. First, the controller has to be able to track the detected phase information without delay, for otherwise the frequency ramp signal may not be generated in time, causing the ILM state to fail to be locked. Second, the increasing rate of the ramp signal needs to be large enough to avoid the escaping effect. Third, the ILM's basin of attraction needs to be large enough so as to generate a finite probability that the MEM array system can enter the basin in response to the rapid frequency ramping.

We now describe a strategy for choosing the control parameters. First, the nonlinear dynamical properties of the MEM array system, which include the typical escaping time of small-amplitude ILMs, phase values of different states, and the size of the ILM basin of attraction, etc., need to be

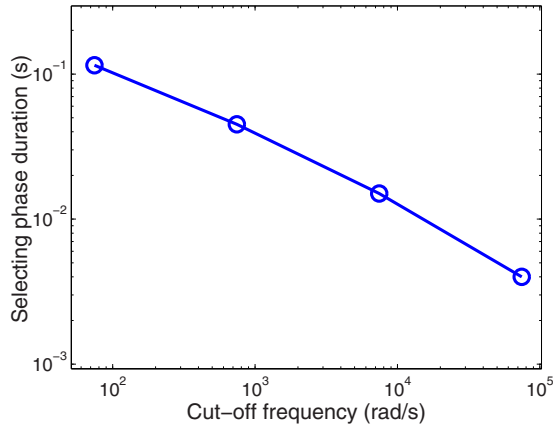

FIG. 6. (Color online) Selection time (defined in Fig. 4) vs the cut-off frequency of the LPF in a MEM array system of size $N=50$.

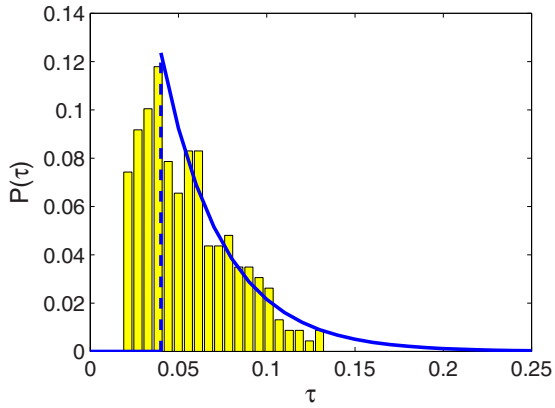

FIG. 7. (Color online) Statistical distribution of transient time τ from Monte Carlo simulations of 6000 trials. The system has $N=128$ beams with the same experiment-based structural parameters as in Fig. 2. The solid curve is a prediction from the Markov model, which holds for τ greater than some nonzero value.

assessed through numerical simulations of the physical model of the system.[15,32] System parameters can then be chosen to satisfy the three conditions mentioned above. In particular, for the first condition, the bandwidth of the LPF in Eq. (3) needs to be large enough to cover the variational rate of the phase signal so as to guarantee that the variable ξ can follow the phase signal in time, as suggested by Eq. (6). However, the bandwidth of the LPF cannot be arbitrarily large because the high-frequency component of the multiplied signal, as shown in Eq. (3), should be effectively filtered. Should this not be the case, the residual high-frequency signal will be coupled to the driven signal, generating phase noise. To illustrate the effect of LPF bandwidth on ILM control, we perform simulations for MEM array system of size $N=50$ by varying the cut-off frequency in Eq. (3). The results are shown in Fig. 6. It can be seen that the duration of phase selection defined in Fig. 4 decreases as the cut-off frequency is increased in a power-law manner. This suggests that, if the bandwidth is small, the ramp signal may not be generated before ILM disappears at the desirable site and the selecting time of the control can be impractically long. After fixing the value of τ, which is inversely proportional to the cut-off frequency, one can choose the amplification gains γ_1 and γ_2 to satisfy the remaining two conditions. To do this, we need to estimate the available range of the slope of the generated frequency ramp signal based on the simulation results of the average escaping time and the size of the ILM's basin of attraction. By adjusting the values of γ_1 and γ_2, we can choose the slope within the estimated range.

IV. TRANSIENT TIME PRECEDING CONTROL

We see that in order to excite an ILM state at a target site, the system has to go through a period of transient phase during which it switches between some spatiotemporal chaotic and low-energy motions. Due to chaos, for different initial conditions, the transient time can be quite different. A relevant issue concerns then the average length of the transient time. Here, we shall construct a Markov model with inputs from numerical computations to characterize the transient phase.

Figure 7 shows the distribution of the transient time for a system of $N=128$ beams (with the same experiment-based structural parameters as in Fig. 2). To generate the statistical distribution, Monte Carlo simulations of 6000 trials are used. In general, the selecting time τ comprises two components: $\tau=\tau_1+\tau_2$, where τ_1 represents the transient time for the system to be in either spatiotemporally chaotic or low-energy state and τ_2 is the switching time. In the following, we discuss the characteristics of τ_1 and τ_2.

Consider a time period during which the system state transits from spatiotemporal chaos to a low-energy state and then back to chaos. We call this time period one iteration. Let ΔT be the average time for one iteration and P be the probability for the system to be excited to an ILM state. The dynamics of the system with respect to the occurrence of ILM can thus be described by a Markov model, as shown in Fig. 8. Note that the probability of transition from a low-energy state to spatiotemporal chaos is unity because of the condition $\dot{\bar{\Omega}}_c<0$ when the system is in a low-energy state.

Since ΔT is small, the probability distribution of random variable τ_2 can be modeled as

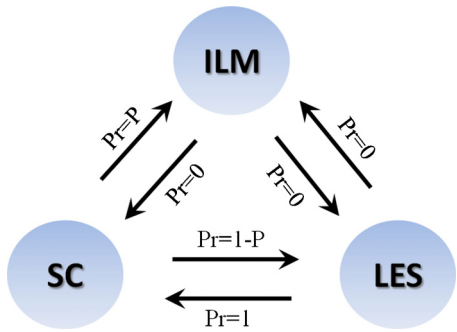

FIG. 8. (Color online) Markov model describing the transient phase of ILM excitation. The probabilities for the system to go from spatiotemporal chaos to an ILM state and to a low-energy state are P and $(1-P)$, respectively. The probability for the system to transit from a low-energy state to spatiotemporal chaos is 1.

$$P_r(\tau_2 = T_2) \approx (1-P)^{T_2/\Delta T-1}P. \quad (27)$$

Due to chaos, τ_1 and τ_2 are effectively independent of each other, so the joint probability distribution for τ_1 and τ_2 is

$$P_r(\tau_1 = T_1, \tau_2 = T_2) \approx P_r{}^{\tau_1}(T_1)(1-P)^{T_2/\Delta T-1}P. \quad (28)$$

We thus have

$$P_r(\tau_1 + \tau_2 = T) \approx (1-P)^{T/\Delta T-1}P \times \int_0^T P_r{}^{\tau_1}(T_1)(1-P)^{-T_1/\Delta T}dT_1. \quad (29)$$

To provide a heuristic explanation for the approximately exponential decay of $P_r(\tau)$, we assume that the distribution of τ_1 has a high peak around its average value: $P_r{}^{\tau_1}(T_1) \approx \delta(T_1 - T_1')$. This leads to

$$P_r(\tau = T) = \begin{cases} P(1-P)^{(T-T_1')/\Delta T-1}, & T \geq T_1' \\ 0, & T < T_1'. \end{cases} \quad (30)$$

This function has a discontinuity of size $P>0$ at $T=T_1'$ but it decreases exponentially for $T>T_1$. The predicted distribution (30) is shown as the solid curve in Fig. 7. The values of the fitting parameters in Eq. (30), i.e., P, T_1', and ΔT can be estimated from the numerical data. For this specific example, to compare with the numerically obtained distribution, we fix $T_1' \approx 0.072$ s, the point of the largest probability in the distribution, and the parameter P is chosen as the probability at $T_1'=0.04$ s. We obtain $P \approx 0.11$. The parameter ΔT can be estimated by the mean value of the iteration period, $\Delta T \approx 0.004$ s, which can be obtained by the time series of Θ_M. Overall, the predicted distribution is consistent with the numerical result.

V. CONCLUSION

In summary, we have proposed a method based on global control to excite ILMs at arbitrarily given sites in MEM oscillator-array systems. Our idea is to take advantage of the spatial heterogeneity and temporal irregularity offered by spatiotemporal chaos and to exploit a typical phase modulation scheme to drive the system in a spatiotemporally chaotic state into the basin of an ILM state. Due to the ubiquity of nonlinear dynamics and chaos in spatially extended systems, we expect our method to be generally applicable to other classes of small-scale devices such as parametrically driven MEM arrays where locally pinning excitations are not feasible.[34] A possible experimental scheme to realize our strategy is phase-locked loops (PLLs),[35] a basic component in many circuit applications. In particular, we can set the initial frequency and phase, respectively, as the reference and the phase angle of the voltage-controlled oscillator, a central component of any PLL circuit. The output of the PLL can then be used to drive the MEM system.

ACKNOWLEDGMENTS

This work was supported by the AFOSR under Grant No. F9550-09-1-0260.

APPENDIX: PHASE ANGLE ASSOCIATED WITH HIGH-ENERGY STATE IN A SINGLE CANTILEVER SYSTEM

Using the classical averaging method,[31] we can obtain an expression for the amplitude and phase of a single MEM resonator as follows:

$$\frac{dr}{dt} = \frac{1}{2\Omega}\left[-\frac{\Omega b r}{m} - \alpha \sin\theta\right],$$

$$\frac{d\theta}{dt} = \frac{1}{2\Omega r}\left[(k_2/m - \Omega^2)r + \frac{3k_4 r^3}{4m} - \alpha\cos\theta\right] \quad (A1)$$

from which we can get the following equations for the amplitude (r) and phase (θ):

$$\left[\left((\Omega_0^2 - k2/m) - \frac{3}{4}\frac{k_4}{m}H\right)^2 + \frac{\Omega^2 b^2}{m^2}\right]H = \alpha^2, \quad (A2)$$

where $H=r^2$ and

$$\left(\frac{3k_4 m^2\alpha^3}{4b^3} - \frac{\Omega^2(m\Omega^2 - k_2)\alpha}{b}\right)\tan\phi^3 + \Omega^3\alpha\tan\phi^2 - \frac{\Omega^2(m\Omega^2 - k_2)\alpha}{b}\tan\phi + \Omega^3\alpha = 0. \quad (A3)$$

We thus have

$$\frac{dH}{d\Omega^2} = \frac{24k_4/mH^2 - 16(\Omega^2 - k_2/m)H}{27k_4^2/m^2H^2 - 3k_4/m(\Omega^2 - k_2/m)H + (\Omega^2 - k_2/m)^2}. \quad (A4)$$

Setting $dH/d\Omega^2=0$, we obtain $\Omega^2=k2/m+3k_4H/(4m)$. Inserting this result into the right-hand side of the second equation of Eq. (A1) and using $d\theta/dt=0$, we get $\cos(\theta)=0$ and, consequently,

$$\theta_{\text{opt}} = -\pi/2. \quad (A5)$$

[1] S. A. Kiselev, S. R. Bickham, and A. J. Sievers, Comments Condens. Matter Phys. **17**, 135 (1995).
[2] S. Flach and C. R. Willis, Phys. Rep. **295**, 181 (1998).
[3] R. Lai and A. J. Sievers, Phys. Rep. **314**, 147 (1999).
[4] P. G. Kevrekidis, K. Rasmussen, and A. R. Bishop, Int. J. Mod. Phys. B **15**, 2833 (2001).
[5] P. Binder, D. Abraimov, A. V. Ustinov, S. Flach, and Y. Zolotaryuk, Phys. Rev. Lett. **84**, 745 (2000).
[6] R. Morandotti, U. Peschel, J. S. Aitchison, H. S. Eisenberg, and Y. Silberberg, Phys. Rev. Lett. **83**, 2726 (1999).
[7] S. F. Mingaleev and Y. S. Kivshar, Phys. Rev. Lett. **86**, 5474 (2001).
[8] M. Sato and A. J. Sievers, Nature (London) **432**, 486 (2004).
[9] A. Smerzi, S. Fantoni, S. Giovanazzi, and S. R. Shenoy, Phys. Rev. Lett. **79**, 4950 (1997); G. J. Milburn, J. Corney, E. M. Wright, and D. F. Walls, Phys. Rev. A **55**, 4318 (1997); I. Zapata, F. Sols, and A. Leggett, *ibid.* **57**, R28 (1998).
[10] S. Zhang and F. Wang, Phys. Lett. A **279**, 231 (2001).
[11] F. Kh. Abdullaev, B. B. Baizakov, S. A. Darmanyan, V. V. Konotop, and M. Salerno, Phys. Rev. A **64**, 043606 (2001).
[12] R. Carretero-González and K. Promislow, Phys. Rev. A **66**, 033610 (2002).
[13] F. Kh. Abdullaev and V. V. Konotop, Phys. Rev. A **68**, 013605 (2003).
[14] L. Roberto, F. Roberto, and O. Gian-Luca, Phys. Rev. Lett. **97**, 060401 (2006).
[15] M. Sato, B. E. Hubbard, and A. J. Sievers, Rev. Mod. Phys. **78**, 137 (2006).
[16] A. Trombettoni and A. Smerzi, Phys. Rev. Lett. **86**, 2353 (2001).

[17]M. Sato, B. E. Hubbard, A. J. Sievers, B. Ilic, D. A. Czaplewski, and H. G. Craighead, Phys. Rev. Lett. **90**, 044102 (2003).
[18]S. Flach and A. V. Gorbachb, Phys. Rep. **467**, 1 (2008).
[19]Q. Chen, L. Huang, and Y.-C. Lai, Appl. Phys. Lett. **92**, 241914 (2008).
[20]M. Sato, B. E. Hubbard, A. J. Sievers, B. Ilic, and H. G. Craighead, Europhys. Lett. **66**, 318 (2004).
[21]Q.-F. Chen, Y.-C. Lai, and D. Dietz, Appl. Phys. Lett. **95**, 094102 (2009).
[22]I. Daumont, T. Dauxois, and M. Peyrard, Nonlinearity **10**, 617 (1997).
[23]D. Bonart and J. B. Page, Phys. Rev. E **60**, R1134 (1999).
[24]This is similar in spirit to the Ott–Grebogi–Yorke scheme of controlling chaos in dynamical systems, where one makes use of the fact that a chaotic set has embedded within itself an infinite number of unstable periodic orbits, and any one of these can, in principle, be stabilized by using small control [E. Ott, C. Grebogi, and J. A. Yorke, Phys. Rev. Lett. **64**, 1196 (1990)].
[25]B. Yurke, D. S. Greywall, A. N. Pargellis, and P. A. Busch, Phys. Rev. A **51**, 4211 (1995).
[26]The phase angle of the oscillation is always negative due to the delay between the output and the input. The low-amplitude oscillation state in the bistable regime is out of phase with respect to the driving force and has a phase angle smaller than $-\pi/2$. The high-amplitude state is in phase with the driving force, with phase angle larger than $-\pi/2$. The maximum-amplitude oscillation has the phase angle exactly equal to $-\pi/2$.
[27]J. J. D'Azzo and C. H. Houpis, *Linear Control System Analysis and Design—Conventional and Modern*, 4th ed. (McGraw-Hill, New York, 1995).
[28]S. Aubry, Physica D **103**, 201 (1997).
[29]R. S. MacKay and S. Aubry, Nonlinearity **7**, 1623 (1994).
[30]P. Maniadis and S. Flach, Europhys. Lett. **74**, 452 (2006).
[31]J. Guckenheimer and P. Holmes, *Nonlinear Oscillations, Dynamical Systems, and Bifurcations of Vector Fields* (Springer, New York, 1990).
[32]Q. Chen, L. Huang, Y.-C. Lai, and D. Dietz, Chaos **19**, 013127 (2009).
[33]This is due to that the spatiotemporal chaotic state is formed by the backbones of ILM saddles, which are high-energy states (Ref. 32). When the orbit wanders around them to form chaotic attractor, the oscillation energy of the time series is typically high.
[34]E. Buks and M. L. Roukes, J. Microelectromech. Syst. **11**, 802 (2002).
[35]P. V. Brennan, *Phase-Locked Loops: Principles and Practice* (McGraw-Hill, London, 1996).